

Mechanical Characterisation of Polyurethane Elastomer for Biomedical Applications

V. Kanyanta and A. Ivankovic

School of Electrical, Electronics and Mechanical Engineering, University College Dublin, Ireland.

1. Introduction

Polyurethane elastomers have been widely used as biomaterials, with applications ranging from medical devices and utilities like cardiac-assist pumps and blood bags, to chronic implants such as heart valves and vascular grafts (Gogolewski, 1992; Christenson et al., 2005; Lelah et al., 1986; Szycher et al., 1992; Stokes et al., 1995; Gunatillake et al., 2003). They were first proposed for use as biomaterials in 1967 by Boretos and Pierce (1967). Their superior mechanical properties and blood compatibility has favored their use and development as biomaterials, particularly as components of implanted devices (Lamba et al., 1997). Polyurethane elastomers offer superior mechanical properties over silicone elastomers, particularly in relation to tear and abrasion, and flex-fatigue life (Wiggins et al., 2003). The chemical composition of these elastomers offers substantial opportunities to synthetic polymer chemists to tailor the structures to meet specific requirements. Generally polyurethanes offer good compatibility with tissue and blood, with a good resistance to mechanical degradation. Thermoplastic polyurethane elastomers are a class of linear segmented copolymers characterised by the presence of urethane (carbamate) groups. They are prepared from three components: a diisocyanate, a macrodiol, and a chain extender (Gunatillake et al., 2003), and can be categorised into two major groups depending on the macrodiol used i.e. ester based or ether based polyurethane (Knoerr and Hoffmann; Recker, 2001). Much research and developments have been done in achieving polyurethanes with excellent biostability with a combination of good mechanical properties and biocompatibility. Polyurethanes used in chronic implants are subject to hostile *in vivo* conditions which can lead to their failure (Stokes et al., 1995; Wiggins et al., 2003;

25 Thoma, 1987; Schmidt et al., 1998; Zhao et al., 1990, 1991; Wu et al., 1992; Schubert et al., 1995,
26 1997).

27 In the current work, an ether based polyurethane elastomer supplied by Renier Technology Ltd (UK)
28 is used for mock arteries, representing large arteries. Like most biological materials, the arterial wall
29 has a very complex mechanical behaviour. It exhibits strong mechanical anisotropy, nonlinear
30 stress-strain behaviour, viscoelasticity and poroelasticity (Julia et al., 1966; L'Italien et al., 1994). Its
31 stress-strain behaviour is also dependent on local hemodynamics and shear stress (Stephanie et al.,
32 1998; Glagov, 1994; Barbee et al., 1994; Tronc et al., 1996), age and inactivity (Vaitkevicious et al.,
33 1993; Kelly et al., 1989; Avolio et al., 1985), pathological infections (David et al., 2002) and high
34 blood pressure (Avolio et al., 1985), and vary widely along the arterial tree (Mangel et al., 1996).

35 The arterial wall is composed of the elastin, vascular smooth muscle cells (VSMC) and connective
36 tissue (Figure 1). Inside, the wall is covered by a monolayer of endothelial cells and epithelial cells
37 form its outside. Due to the complex structure and behavior, it is extremely difficult to find a
38 material with similar mechanical behaviour to arteries or to model it by a single hyperelastic
39 material model. Although the properties of polyurethane elastomer differ from those of the arteries,
40 it was chosen because of its good biocompatibility and viscoelastic properties, and for its wide use
41 in vascular grafts (Szycher, 1998; Gunatillake et al., 2003), making it a preferred material for mock
42 arteries in this work.

43 Since constitutive material models can not entirely describe the stress-strain behaviour of the
44 material under all loading conditions due to enormous variations and complexity involved, material
45 tests were designed based on loading conditions representative of the application of interest. These
46 conditions were chosen to be representative of *in vivo* loading conditions of large arteries. Material
47 tests included uniaxial tests under varying temperature, humidity and strain rates, planar and
48 equibiaxial tension, relaxation, creep and cyclic tests on specimens made of polyurethane elastomer.
49 Cyclic tests were performed to establish viscoelastic properties of the elastomer relevant for

50 pulsatile pressure loading of mock arteries. Also performed were static and dynamic flow tests on
51 polyurethane tubular specimens representing mock arteries, which are discussed in detail in (Quinn
52 et al., 2008).

53 Although polyurethane elastomer is widely used, its mechanical behaviour has never been
54 extensively characterised. The material properties of the elastomer are usually measured in uniaxial
55 tension only, under dry room temperature and at low strain rates (Diaconu et al., 2006; Pathiraja et
56 al., 1996; Diaconu et al., 2005). This work establishes the variations in the behaviour of
57 polyurethane elastomer with temperature, humidity and strain rate and also reports planar and
58 equibiaxial tension, relaxation, creep and cyclic test results, providing a comprehensive
59 characterisation of polyurethane elastomer.

60 This work is part of the study looking at the role of hemodynamic shear stress in atherosclerosis,
61 by predicting accurately the distribution and rate of change of wall shear stress in various arterial
62 geometries (straight and branched mock arteries) and establishing the role of arterial flexibility on
63 wall shear stress.

64 **2. Test Methods**

65 Material tests performed on polyurethane elastomer specimens included uniaxial, planar and
66 equibiaxial tension, stress relaxation, creep and cyclic loading. The test specimens were of different
67 geometries (Figure 2), according to the test being performed. All the stresses and strains presented in
68 the plots in this work refer to the engineering stress and strain, respectively.

69 **2.1. Uniaxial Tension**

70 Uniaxial tension tests were performed using dumbbell shaped specimens (Figure 2(a)). These
71 tests can be divided into three groups, according to the strain rates employed i.e. low ($< 1/s$),
72 intermediate (between $1/s$ and $100/s$) and high ($> 100/s$) strain rate uniaxial tension tests.

73 Low strain rate tests were performed under three different conditions; dry-room temperature,
74 wet-room temperature and wet@37°C, on a standard Instron machine. A laser extensometer was
75 used for a non contact measurement of strains. This is important when measuring strains of soft
76 materials as any strain measurement involving contact could affect the stiffness of the specimen. An
77 environmental chamber, equipped with a thermostat controlled heater, was used to maintain the test
78 temperature constant (e.g. 37 °C for wet@37 °C condition) for the duration of the test. Specimens
79 were submerged in water at the set temperature for one hour prior to testing, and remained
80 submerged for the duration of the test.

81 Intermediate and high strain rate uniaxial tests were performed under dry-room temperature
82 condition only, due to the current experimental limitations. An instrumented drop-weight tester
83 (Figure 3) and split Hopkinson pressure bar in tension (Figure 4) were used for intermediate and
84 high strain rate uniaxial tests, respectively.

85 For intermediate strain rate tests, load measurements were achieved with a calibrated strain gage,
86 while specimen strains were obtained from the displacement of the striker (Figure 3), with the zero
87 position defined as the point of initial contact between the striker and the impact plate.

88 Under high strain rate tests (Figure 4), a swinging pendulum was used to load the specimens.
89 When the pendulum striker hits the block, a tensile stress pulse is generated in the incident bar. A
90 dumbbell shaped cylindrical fracture piece made of Perspex (2.5 mm in diameter) breaks on impact,
91 thus, preventing multiple pulses being generated. The amplitude of the generated pulse is equal to
92 stress required to break the fracture piece, which in this case corresponds to a stress of 1.4 MPa and
93 57 MPa in the incident bar and fracture piece, respectively. In this way the amplitude of the incident
94 pulse can be controlled by varying the diameter of the fracture piece (Shim et al., 2001). The
95 generated tensile pulse propagates through the incident bar into the specimen. At the bar-specimen
96 interface, part of this pulse is transmitted into the specimen and propagates through the transmitter

97 bar as a tensile pulse. The rest of the pulse reflects into the incident bar as a compressive pulse. The
 98 transmitted and reflected pulses are recorded by the transmitter and incident strain gages,
 99 respectively.

100 Specimen stress σ and strain ϵ are obtained from the transmitted and reflected strain
 101 signals, respectively, using the classical Kolsky analysis given by

$$102 \quad \sigma = \frac{E_b A_b}{A_s} \left(\frac{1}{l_s} \int_0^{l_s} \epsilon_t dx - \frac{1}{l_s} \int_0^{l_s} \epsilon_r dx \right) \quad (1a)$$

$$103 \quad \epsilon = \frac{A_b}{A_s} \left(\frac{1}{l_s} \int_0^{l_s} \epsilon_t dx + \frac{1}{l_s} \int_0^{l_s} \epsilon_r dx \right) \quad (1b)$$

104 where A_b and A_s are the bar and specimen cross-section areas respectively, ϵ_t is the transmitted
 105 strain signal, ϵ_r is the reflected strain signal, l_s is the specimen gage length and C_b is the wave speed
 106 through the bar (i.e. $C_b = \sqrt{E_b/\rho}$). The material used for the incident and transmitter bars was a
 107 Glass Filled Nylon 66 with a Young's modulus $E = 13.2GPa$, density $\rho = 1460 \text{ Kg/m}^3$, and diameter
 108 $D = 16mm$.

109 Ten specimens were tested at each strain rate for low strain rate uniaxial tests and five
 110 specimens at each strain rate for intermediate and high strain rate uniaxial tests.

111 2.2. Choice of Maximum Loading Rate

112 A maximum strain rate for the tests was chosen as the upper limit of the range of strain rates
 113 experienced by arteries *in vivo*. Strain rates in arteries can be estimated analytically, numerically or
 114 experimentally if the pressure waveform and arterial wall properties are known. The average
 115 Young's modulus for the arterial wall is reported to range between 600kPa and 1MPa (Riley et al.,
 116 1992). Taking for instance the pressure waveform for the carotid artery (Figure 5(a)) (Augst et al.,
 117 2007), strain rates, $\dot{\epsilon}_h = d(pd/2Eb)/dt$, in the artery can be estimated as shown in Figure 5(b)
 118 (assuming the artery's internal diameter $d = 10mm$, thickness $b = 1mm$ and Young's modulus $E =$

119 800kPa. p is the pressure). Therefore, the maximum strain rates in arteries can be assumed to be
120 about 1/s. However, strain rates of up to 175/s were used in the design of uniaxial tension tests in
121 order to fully establish the strain rate behaviour of polyurethane rubber, although this may not be
122 particularly necessary for the current study.

123 **2.3. Uniaxial Stress relaxation and Creep**

124 Creep tests were performed by holding a specimen at a constant tensile stress and measuring the
125 resulting strain ϵ as a function of time. Similarly, relaxation tests were performed by holding a
126 specimen at a constant tensile strain and measuring the resulting stress σ as a function of time. Stress
127 (for creep tests) and strain (for relaxation tests) were automatically controlled by use of QMAT
128 Materials Testing and Analysis Software.

129 Two stress magnitudes, 0.44 MPa and 1.136 MPa, were used for creep tests and four strain
130 magnitudes, 5%, 6.5%, 8% and 10%, for stress relaxation tests. Five specimens were tested at each
131 stress or strain magnitude. Material stress relaxation and creep were allowed for 2000s in each case.

132 **2.4. Uniaxial Cyclic Tests**

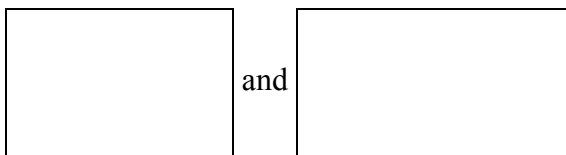
133 Under uniaxial cyclic loading, the loading of the specimens was periodically repeated over 10
134 cycles. The loading function was either force (stress) or displacement (strain), which repeatedly took
135 the form of equation (2). Constant triangular stress or strain cycles were applied, while the other
136 quantity (strain or stress) is allowed to vary according to material behaviour (Sandor, 1972). The
137 experimental set-up is similar to uniaxial tension tests and dumbbell shaped specimens (Figure 2(a))
138 were used. Four specimens were tested with either stress or strain as a loading function, making a
139 total of eight specimens. Tests were performed at a loading rate of 10mm/min (corresponding to a
140 strain rate of 0.013/s), under dry-room temperature condition.

$$141 \quad \epsilon(t), \sigma(t) = a * \begin{cases} t; & 0 \leq t \leq T/2 \\ T-t & T/2 \leq t \leq T \end{cases}, \quad (2)$$

142 where “a” is the loading rate (strain or stress per unit time) and “T” is the period of the triangular
143 function.

144 2.5. Planar tension

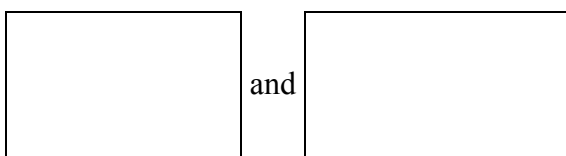
145 Specimens used for the planar tension tests were 6 times wider than their gage length (Figure
146 2(b)). This was in order to achieve a deformation, F , and stress, σ , state given by (assuming the
147 elastomer behaves as an incompressible material)

148  (3)

149 The material is constrained in the transverse direction and only deforms in the loading and thickness
150 directions (Miller, 1999). Apart from a different specimen type, the experimental set-up is the same
151 as for simple tension. Tests were conducted under dry-room temperature condition at a strain rate of
152 0.013/s.

153 2.6. Equibiaxial tension

154 Cruciform type specimens (Figure 2(c)) were used for equibiaxial tension tests. The
155 experimental set-up is as shown in Figure 6. The material was loaded in both directions, at a
156 constant strain rate of 0.013/s, in such a way that the stretches in the two loading directions are
157 identical i.e. λ . This was achieved by using a system of pulleys shown in Figure 6(b). The
158 specimen deformation, F , and stress, σ , state are

159  (4)

160 Load measurements were achieved with the Load cell while specimen strains were obtained from
 161 the displacement of the cross head. Tests were conducted under dry-room temperature condition,
 162 and stress and strain were measured in one direction only.

163 2 mm diameter nylon strings with a Young's modulus of 3.9 GPa were used as connecting
 164 strings (Figure 6(b)). Considering that the maximum load for the tests is in the range of 20-30 N,
 165 deformations in the nylon strings is expected to be insignificant.

166 **3. Hyperelastic Material Models**

167 For isotropic hyperelastic materials, the strain-energy function W can be defined in terms of
 168 strain invariants $I_i (i = 1,2,3)$ or principal stretches $\lambda_i (i = 1,2,3)$ i.e.

$$169 \quad W = W(I_1, I_2, I_3) \quad \text{or} \quad W = W(\lambda_1, \lambda_2, \lambda_3) \quad (5)$$

170 If incompressibility is assumed (i.e. $I_3 = 1$), equation (5) then reduces to a function of two variables
 171 only i.e. I_1 and I_2 . Therefore, for an isotropic, incompressible material, the principal Cauchy stresses
 172 in the loading axis for uniaxial, planar and equibiaxial tension are given by equations 6, 7 and 8,
 173 respectively (Holzapfel, 2000).

$$174 \quad \sigma_{11} = 2 \left(\lambda^2 - \frac{1}{\lambda} \right) \left[\frac{\partial W}{\partial I_1} + \frac{1}{\lambda} \frac{\partial W}{\partial I_2} \right]. \quad (6)$$

$$175 \quad \sigma_{11} = 2 \left(\lambda^2 - \frac{1}{\lambda^2} \right) \left[\frac{\partial W}{\partial I_1} + \frac{\partial W}{\partial I_2} \right]. \quad (7)$$

$$176 \quad \sigma_{11} = \sigma_{22} = 2 \left(\lambda^2 - \frac{1}{\lambda^4} \right) \left[\frac{\partial W}{\partial I_1} + \lambda^2 \frac{\partial W}{\partial I_2} \right]. \quad (8)$$

177 **4. Results**

178 The results of the material tests show the behaviour of the polyurethane elastomer tested to be
 179 highly dependent on temperature and humidity, as shown in Figure 7(a). The elastomer significantly

180 softens with increase in temperature and humidity levels, with the Young's modulus of 7.4 MPa, 5.3
181 MPa and 4.7 MPa for dry-room temperature, wet-room temperature and wet@37°C conditions,
182 respectively. These results agree with the reported observations that polyurethane based medical
183 invasive devices soften significantly within minutes of insertion into a human body, resulting in
184 reduced patient discomfort and risk of vascular trauma (Tilak, 2001). The reported Young's
185 modulus of polyurethane elastomer at dry room temperature varies widely depending on elastomer
186 composition, with values of 3.6 MPa (Diaconu and Dorohoi, 2005), 13.1 MPa (Diaconu et al.,
187 2006), and 14.6 – 88.8 MPa (Pathiraja et al., 1996). All the stresses and strains presented in the plots
188 in this paper refer to the engineering stress and strain, respectively.

189 Figure 7(b) shows the stress-strain behaviour of polyurethane elastomer under uniaxial, planar
190 and equibiaxial tension, for a strain rate of 0.013/s and under dry-room temperature condition. At
191 low strain rates ($< 1/s$), the elastomer shows little or no strain rate dependency (Figure 8). Therefore,
192 under this range of strain rates, the behaviour of polyurethane elastomer can be considered strain
193 rate independent.

194 Intermediate strain rate uniaxial tension test results are presented in Figure 9, for three different
195 strain rates. Under this range of strain rates, polyurethane elastomer shows considerable strain rate
196 sensitivity, with the Young's modulus of 8 MPa, 9.5 MPa and 10.5 MPa for the strain rates of 29.4
197 /s, 58.8 /s and 88.2 /s, respectively. There is significant scatter in the results of the tests at 88.2 /s,
198 above 30% strains (Figure 9(c)). This is probably due to the inaccuracy in conducting these tests as
199 the impact speed increase. However, for strains below 20%, the results are very repeatable for all the
200 three strain rates.

201 Figure 10 presents high strain rate test results for a strain rate of 137.5 /s. The incident and
202 reflected strain signals, recorded by the incident strain gage, are shown in Figure 10(a), while the
203 transmitted strain signals (recorded by the transmitted strain gage) are presented in Figure 10(b).
204 The noise in the transmitted signal is significant because of the high amplification used, owing to the

205 small signal amplitude. The averaged results are shown in Figure 10(c), and the reflected and
206 transmitted strain signals, which are aligned to have a common starting point in time, in Figure
207 10(d).

208 Applying Kolsky analysis (equation (1)) on the transmitted and reflected strain signals yields
209 the stress-strain curves shown in Figure 11, showing the loading phase and part of the unloading
210 phase, for the strain rates of 137.5 /s and 175 /s. The unloading curve does not follow the same path
211 as the loading curve, probably due to the interference in the transmitted signal (Figure 10(c)) caused
212 by the re-reflected waves (resulting in 2nd stage loading of the specimen). The material's Young's
213 modulus at these strain rates is 12 MPa and 13.5 MPa, for 137.5 /s and 175 /s strain rates,
214 respectively. Figure 12 presents the change in the stiffness of polyurethane elastomer with increase
215 in strain rate. The Young's modulus linearly increases with the strain rate at a rate of 0.034 MPa per
216 strain rate.

217 Viscoelastic properties of polyurethane elastomer were determined from stress relaxation and
218 creep tests by fitting a 3-term Prony series to the relaxation and creep data. Figure 13 presents the
219 relaxation and creep data, and the calculated relaxation and creep compliance for different strain and
220 stress magnitudes, respectively. At 2000s, the material can be considered stabilized (when the
221 material modulus reaches a steady-state value) since the difference in the stress at 500s and 2000s is
222 less than 2 % (Figure 14 (a)). The material's relaxed modulus is determined by plotting the relaxed
223 data at 2000s against the strains (Figure 13(e)). This value is 6.5 MPa, and is 88 % of the initial or
224 unrelaxed modulus. The relaxation modulus $E(t)$ and creep compliance $J(t)$ functions, determined by
225 fitting the Prony series to the relaxation data (Figure 14(a)) and creep data (Figure 14(b)),
226 respectively, are given by

227
$$\boxed{\hspace{15em}}$$
 (9a)

228
$$\boxed{\hspace{15em}}$$
 (9b)

229 The averaged uniaxial cyclic test results (for eight specimens) are shown in Figure 15, with
230 stress as a loading function (Figure 15(a)) and strain as a loading function (Figure 15(b)). The results
231 show that the behaviour of polyurethane elastomer under cyclic loading exhibits creep and stress
232 relaxation behaviours similar to those observed under static conditions or monotonic loading (Figure
233 13). When stress is applied as a loading function, the material undergoes creep as it deforms, which
234 follow the same pattern as the creep data at 0.44 MPa constant stress (Figure 15(a)). Similarly, when
235 strain is used as a loading function, the material undergoes stress relaxation (Figure 15(b)). Stress
236 relaxation and creep behaviours in cyclic loading can be described in the same manner as under
237 static conditions. After about 500s (or 10 loading cycles), there is little or no significant changes in
238 the peaks of either stress or strain with successive loading cycles (maximum changes are below 2 %
239 at this point). The material can hence be deemed stabilised after this point.

240 **4.1. Hyperelastic Material Models**

241 In this work, the polyurethane elastomer tested is treated as an isotropic, incompressible
242 material. These assumptions are valid within experimental reason since the material anisotropy is
243 only 10 % and the Poisson ratio ν is 0.475 +/- 0.025 (Kanyanta, 2008). Therefore, isotropic,
244 incompressible hyperelastic material models were used in the choice of a representative material
245 model for the elastomer

246 Six hyperelastic material models were fitted to the uniaxial, planar and equibiaxial tension
247 experimental data using equations 6, 7 and 8, respectively, as shown in Figure 16. The strain energy
248 functions for each material model are given in the appendix.

249 In order to relate the Cauchy stress in equations 6, 7 and 8 to the engineering stress σ_{eng} in
250 experimental results, equation (13) was used.

$$251 \quad \sigma_{11} = \sigma_{eng} \frac{A}{A_f} = \sigma_{eng} \lambda, \quad (13)$$

252 where A and A_f are the original and deformed cross-section areas respectively.

253 Yeoh's model provides the best fit to the range of experimental data (Figure 17(e)), with a R-
254 squared value of 0.996. However, other models such as Neo-Hookean model, can be sufficient if one
255 is only concerned with small strain deformations (below 15 %)

256 **5. Discussion**

257 The effects of humidity and temperature on material properties of polyurethane elastomers are
258 usually not reported. This study presents a comprehensive characterisation of an ether-based
259 polyurethane elastomer and reports the variations in its properties with humidity, temperature and
260 strain rate. The behaviour of the elastomer is highly dependent on humidity, temperature and strain
261 rate, with the Young's modulus of 7.4MPa, 5.3MPa and 4.7MPa, at dry-room temperature, wet-
262 room temperature and wet@37°C, respectively, and at strain rates below 1/s. Thus, the stiffness of
263 polyurethane implants inside a human body is significantly different from that at dry-room
264 temperature. This agrees with earlier observations that polyurethane elastomer products significantly
265 soften on insertion into a human body (Tilak, 2001), thus, reducing a patient's post operation
266 vascular trauma. A similar trend in humidity and temperature dependency behaviour is expected for
267 all grades of polyurethane elastomers due to the strong similarities in their basic chemical structures
268 (Knoerr and Hoffmann; Recker, 2001).

269 The Young's modulus of the elastomer also increased significantly at high strain rates with
270 values of 7.4 MPa, 8 MPa, 9.5 MPa, 10.5 MPa, 12 MPa and 13.5 MPa, at strain rates of <1/s, 29.4/s,
271 58.8/s, 88.2/s, 137.5/s and 175/s, respectively, at dry-room temperature. However, strain rates in
272 arteries are not expected to exceed 2/s (twice the estimated upper bound strain rate, Section 2.2).
273 This also applies to the current study using polyurethane mock arteries. The Young's modulus only
274 varies by about 0.5 % between 1/s and 2/s (Figure 12). Therefore, the Young's modulus at low strain
275 rates (< 1/s) is sufficient to describe the stiffness of the elastomer for the range of strain rates in

276 arteries. Intermediate and high strain rates were only used to fully describe the strain rate dependent
277 behaviour of polyurethane elastomer, but were not particularly necessary in this study.

278 Most literature values for the Young's modulus of polyurethane elastomer are measured at dry-
279 room temperature and low strain rates. These include 3.6 MPa (Diaconu and Dorohoi, 2005), 13.1
280 MPa (Diaconu et al., 2006), and 14.6 – 88.8 MPa (Pathiraja et al., 1996). The wide variation in these
281 values is due to the wide variety in the composition of polyurethane elastomers. These values are not
282 adequate for modeling the behaviour of e.g. polyurethane implants inside a human body (at wet@37
283 deg Celsius) since the stiffness of polyurethane elastomer is seen to be highly dependent on
284 humidity and temperature.

285 Polyurethane elastomer exhibits significant viscoelastic behaviour. Stress relaxation and creep
286 behaviour under cyclic loading also compares well with that seen under monotonic loading. Most
287 importantly is that, under cyclic loading, the elastomer reaches a steady-state behaviour within the
288 first 10 loading cycles. This means that the material properties measured under monotonic loading
289 can be used to model the behaviour of the elastomer under cyclic loading, assuming the material has
290 reached steady-state conditions. The relaxed modulus at dry-room temperature was 14 % (6.5MPa)
291 less than the initial modulus (7.4 MPa). Since creep and relaxation tests could not be conducted at wet-
292 room temperature and wet-37deg Celsius, the same trend in material relaxation is assumed. Future
293 work will clarify this. A 3-term Prony series was sufficient to model the elastomer's viscoelastic
294 behaviour (Figure 14).

295 The elastomer also exhibits 10 % anisotropy and its Poisson ratio ranged between 0.45 - 0.5. In
296 the current study, 10 % anisotropy is deemed insignificant and the Poisson ratio is treated to be close
297 enough to 0.5. Therefore, the elastomer is assumed as an isotropic, incompressible material, and
298 standard isotropic, incompressible hyperelastic material models are used in the choice of a
299 representative material model for the elastomer. Yeoh's model was found to be the best
300 representative material model for this elastomer. However, other models such as Neo-Hookean

301 model, which is much simpler to implement in numerical codes, can be sufficient if one is only
302 concerned with small strain deformations (below 15 %).

303 The chemical and bio-stability of the elastomer was not examined in this study. This is
304 adequately covered in literature (Stokes et al., 1995; Wiggins et al., 2003; Thoma, 1987; Schmidt et
305 al., 1998; Zhao et al., 1990, 1991; Wu et al., 1992; Schubert et al., 1995, 1997).

306 **6. Conclusion**

307 The behaviour of the ether-based polyurethane elastomer tested is humidity, temperature and strain
308 rate dependent. Its Young's modulus is almost 40% less at wet@37 deg Celsius than it is at dry-
309 room temperature, and linearly increases with increase in strain rate at a rate of 0.034 MPa/strain
310 rate. For the range of strain rates found in arteries, i.e. 0 – 4 /s, there is insignificant variation in the
311 Young's modulus of the elastomer and, thus, the Young's modulus can be assumed constant. The
312 elastomer also exhibits 10 % anisotropy and 13 % viscoelasticity. The Yeoh model is the best
313 representative material model for this elastomer, over a range of strains up to 300 %.

314 Although there is a wide variety of polyurethane elastomers used as biomaterials, the trend in
315 their humidity and temperature dependency and cyclic and viscoelastic behaviour are expected to be
316 very similar. Therefore, material properties measured at dry-room temperature can not be taken as
317 the properties for polyurethanes used for chronic implants at wet@37 deg Celsius. Therefore, it is
318 important that the properties of the elastomer are measured at conditions mimicking those of the
319 intended application.

320

321 **Acknowledgments**

322 The authors wish to thank Science Foundation Ireland for the financial support of this work, and Dr.
323 N. Murphy from UCD for constructive discussions and review of this manuscript.

References

- Andrew, O.M., David, W.H., Marvin, H.S., Richard, N.R., Margot, R.R., 1998. The effect of storage time and repeated measurements on the elastic properties of isolated porcine aortas using high resolution x-ray CT. *J. Physiol. Pharmacol.* 76, 451- 456.
- Augst, A. D., Ariff, B., McG. Thom, S. A. G., et al., 2007. Analysis of complex flow and the relationship between blood pressure, wall shear stress, and intima-media thickness in the human carotid artery. *J Physiology - Heart and Circulatory Physiology*, 293, H 1031-37.
- Avolio, A.P., Deng Fa-Quan, Li Wei-Qiang, Yao-Fei, L., Zhen-Dong, H., Lian-Fen, X., O'rourke, M.F., 1985. Effects of aging on arterial distensibility in populations with high and low prevalence of hypertension: comparison between urban and rural communities in China. *Circulation* 71, 202-10.
- Barbee, K.A., Macarak, E.J., Thibault, L.E., 1994. Strain measurements in cultured vascular smooth muscle cells subjected to mechanical deformation. *Ann Biomed Eng.* 22, 14–22.
- Boretos, J.W., Pierce, S.W., 1967. Segmented Polyurethane: A New Elastomer for Biomedical Applications. *Science* 158, 1481 – 1482.
- Christenson, E.M., Wiggins, M.J., Anderson, J.M., Hiltner, A., 2005. Surface modification of poly(ether urethane urea) with modified dehydroepiandrosterone for improved in vivo biostability. *J Biomed Mater Res* 73A, 108–115.
- David, F.M., Gheona, A., Randall, P., Umberto, C., Julio, A.P., Emilios, D., Raphael, S., 2002. Arterial wall properties and Womersley flow in Fabry disease. *BMC Cardiovascular Disorders*, 2:1.
- Diaconu, I., Dorohoi, D., Topoliceanu, F., 2006. Electrostriction of a polyurethane elastomer-based polyester. *IEE sensors journal* 6, 876-880.
- Diaconu, I., Dorohoi, D., 2005. Properties of polyurethane thin films. *Journal of Optoelectronics and Advanced Materials* 7, 921-924.

- Glagov, S., 1994. Intimal hyperplasia, vascular remodeling, and the restenosis problem. *Circulation* 89, 2888–2891.
- Gogolewski S., 1991. *In vitro* and *in vivo* molecular stability of medical polyurethanes: A review. *Trends Polym Sci* 1, 47–61.
- Greenshields, C.J., Weller, H.G., Ivankovic, A., 1999. The Finite Volume Method for Coupled Fluid Flow and Stress Analysis. *Computational Modeling and Simulation in Engineering* 4, 213-218.
- Gunatillake, P.A., Martin, D.J., Meijs, G.F., et al., 2003. Designing Biostable Polyurethane Elastomers for Biomedical Implants. *Aust. J. Chem.* 56, 545-557.
- Holzapfel, G. A., 2000. *Nonlinear Solid Mechanics, A Continuum Approach for Engineering*. John Wiley & Sons Ltd, England, pp. 222-227.
- Julia, T.A., Murray, R., Dorothy, H.C., 1966. Correlation of Visco-elastic Properties of Large Arteries with Microscopic Structure. *Circulation Research* 19, 104-121.
- Kanyanta, V., 2008. *Towards Early Diagnosis of Atherosclerosis: Wall Shear Stress Prediction*. PhD Thesis, University College Dublin, School of Electrical, Electronics and Mechanical Engineering.
- Karac, A., Ivankovic, A., 2003. Modelling the drop impact behaviour of fluid-filled polyethylene containers. *Fracture of Polymers, Composites and Adhesives II* 32, 253-264. ESIS Publication, Elsevier Ltd.
- Kelly, R., Hayward, C., Avolio, A., O'Rourke, M., 1989. Noninvasive Determination of Age-Related Changes in the Human Arterial Pulse. *Circulation* 80, 1652-59.
- Knoerr, K. and Hoffmann, U., 2001. Millable Polyurethane Elastomers, *Handbook of Elastomers*, 2nd Edition 753-764. Marcel Decker, Inc., New York. Editors: Bhowmick, A. K. and Stephens, H. L.
- Lamba, N.M.K., Woodhouse, K.A., Cooper, S.L., Lelah, M.D., 1997. Polyurethanes in biomedical applications. *CRC Press*, pp 1-3.

- Lelah, M.D., Cooper, S.L., 1986. Polyurethanes in medicine. Boca Raton, FL: CRC Press.
- L'Italien, G. J., Chandrasekar, N. R, Lamuraglia, G. M., Pevec, W. C., Dhara, S., Warnock, D. F., Abbott, W. M., 1994. Biaxial elastic properties of rat arteries in vivo: influence of vascular wall cells on anisotropy. *J Physiol Heart Circ Physiol* 267, H574-H579.
- Maneeratana, K., 2000. Development of the finite volume method for non-linear structural applications. PhD thesis, Imperial College of Science, Technology and Medicine.
- Mangell, P., Lanne, T., Sonesson, B., Hansen, F., Bergqvist, D., 1996. Regional Differences in Mechanical Properties between Major Arteries in an Experimental Study in Sheep. *Eur J Vasc Endovasc Surg* 12, 189-195.
- Miller, K., 1999. Testing elastomers for hyperelastic material models in finite element analysis. *Elastomer Technology International*, p.88.
- O'Dowd, N.P., Knauss, W.G., 1995. Time dependent large principal deformation of polymers. *Mech. Phys. Solids* 43, 771-792.
- Pathiraja, A.G., Gordon, F.M., Simon, J.M., Nicole, S., 1996. Polyurethane elastomers with low modulus and hardness based on novel copolyether macrodiols. *J Appl Polym Sci* 63, 1373-1384.
- Quinn, N and Ivankovic, A., 2009. Towards Early Diagnosis of Atherosclerosis: The effect of thickening and stiffening on the deformation profiles of polyurethane mock arteries. In preparation.
- Recker, K., 2001. Cast Polyurethane Elastomers, *Handbook of Elastomers*, 2nd Edition 765-774. Marcel Decker, Inc., New York. Editors: Bhowmick, A. K. and Stephens, H. L.
- Riley, W.A., Barnes, R.W., Evans, G.W., et al., 1992. Ultrasonic Measurement of the Elastic Modulus of the Common Carotid Artery. *The Atherosclerosis Risk in Communities (ARIC) Study*. *Stroke* 23, 952-956.

- Rivlin, R.S., 2004. A note on the constitutive equation for an Isotropic Elastic Material. *Mathematics and Mechanics of Solids* 9, 121-129.
- Sandor, B.I., 1972. *Cyclic stress and strain*. University of Wisconsin Press.
- Schmidt, J.A., Stotts, L.J., 1998. Bipolar pacemaker leads: new materials, new technology. *J Invest Surg* 11, 75– 81.
- Schubert, M., Wiggins, M., Schaefer, M., et al., 1995. Oxidative biodegradation mechanisms of biaxially strained poly(ether urethane urea) elastomers. *J Biomed Mater Res* 29, 337–347.
- Schubert, M., Wiggins, M., Anderson, J., et al., 1997. Role of oxygen in biodegradation of poly(ether urethane urea) elastomers. *J Biomed Mater Res* 34, 519–530.
- Shim, V. P. W., Yuan, J., Lee, S. H., 2001. A Technique for Rapid Two-stage Dynamic Tensile Loading of Polymers. *Experimental Mechanics* 41, 122-127.
- Stéphanie, L., Alain, T., 1998. Signal Transduction of Mechanical Stresses in the Vascular Wall. *Hypertension* 32, 338-345.
- Stokes, K., McVenes, R., 1995. Polyurethane elastomer biostability. *J Biomater Appl* 9, 321–354.
- Szycher, M., Reed A., 1992. Biostable polyurethane elastomers. *Med Device Technol* 3:42–51.
- Szycher, M., 1998. Polyurethanes in vascular grafts. *Elastomer World*, April 1.
- Tilak M. Shah, 2001. Dip molding of polyurethane and silicone for latex-free nonallergic products. *Medical Device and Diagnostic Industry*.
- Tronc, F., Wassef, M., Esposito, B., Henrion, D., Glagov, S., Tedgui, A., 1996. Role of NO in flow-induced remodeling of the rabbit common carotid artery. *Arterioscler Thromb Vasc Biol.* 16, 1256–1262.
- Thoma, R.J., 1987. Poly(ether) urethane reactivity with metal-ion in calcification and environmental stress cracking. *J Biomater Appl* 1, 449–462.
- Tzikang Chen, 2000. Determining a Prony series for a viscoelastic material from time varying strain data. NASA/TM-2000-210123.

- Vaitkevicius, P.V., Fleg, J.L., Engel, J.H., O'Connor, F.C., Wright, J.G., Lakattam, L.E., Yin, F.C.P., Lakatta, E.G., 1993. Effects of Age and Aerobic Capacity on Arterial Stiffness in Healthy Adults. *Circulation* 88, 1456-62.
- Wiggins, M.J., Anderson, J.M., Hiltner, A., 2003. Effect of strain and strain rate on fatigue-accelerated biodegradation of polyurethanes. *J Biomed Mater Res* 66A, 463–475.
- Wu, Y., Sellitti, C., Anderson, J., et al., 1992. An FTIR-ATR investigation of in vivo poly(ether urethane) degradation. *J Appl Polym Sci* 46, 201–11.
- Zhao, Q., Agger, M.P., Fitzpatrick, M., et al., 1990. Cellular interaction with biomaterials: in vivo cracking of pre-stressed Pellethane 2362-80A. *J Biomed Mater Res* 24, 621–637.
- Zhao, Q., Topham, N., Anderson, J.M., et al., 1991. Foreign-body giant cells and polyurethane biostability: *in vivo* correlation of cell adhesion and surface cracking. *J Biomed Mater Res* 25, 177–183.

Appendix

Hyperelastic material models and their strain energy functions

NeoHookean: , μ is the shear modulus.

2-term Mooney Rivlin: .

3-term Mooney Rivlin: .

Arruda-Boyce: .

where .

Yeoh:
$$W = \sum_{i=1}^3 C_i (I_1 - 3)^i.$$

Ogden:
$$W = \sum_{i=1}^n \frac{\mu_i}{\alpha_i} (\lambda_1^{\alpha_i} + \lambda_2^{\alpha_i} + \lambda_3^{\alpha_i} - 3) \quad n = 3.$$

Figures

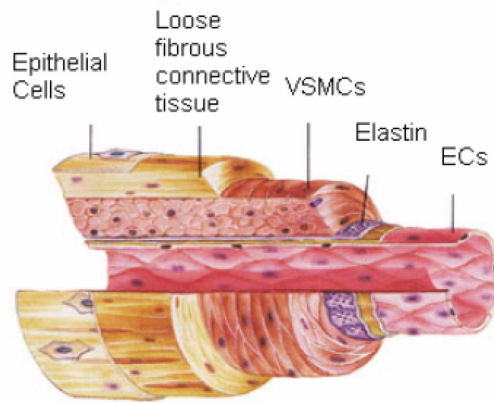


Figure 1: Arterial wall composition.

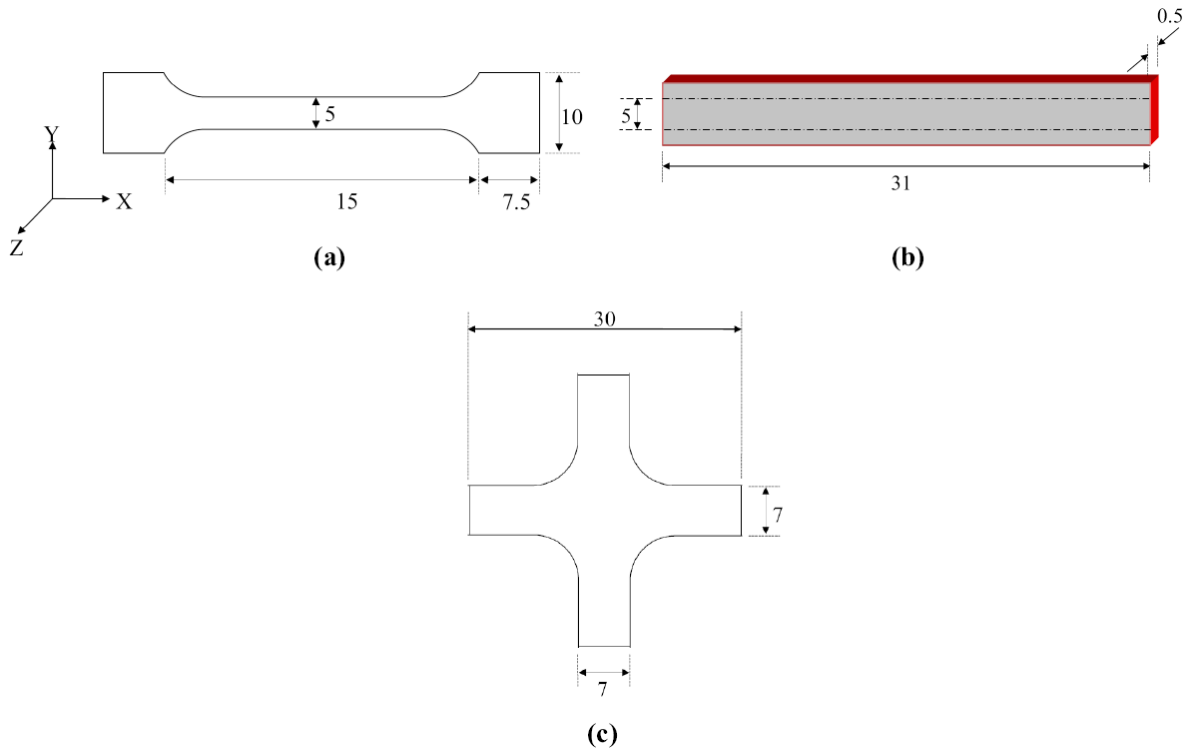


Figure 2: Specimen geometries for (a) uniaxial tension, cyclic, stress relaxation and creep, (b) planar tension and (c) biaxial tension tests. All dimensions are in mm

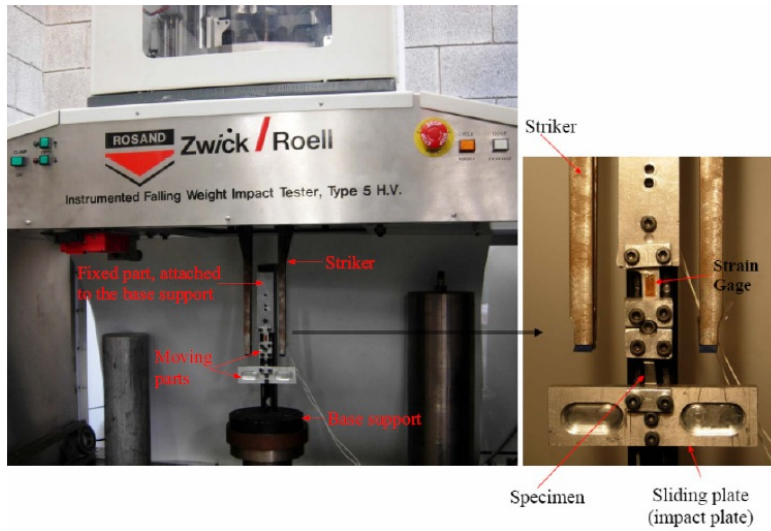


Figure 3: Experimental set-up for intermediate strain rate tests

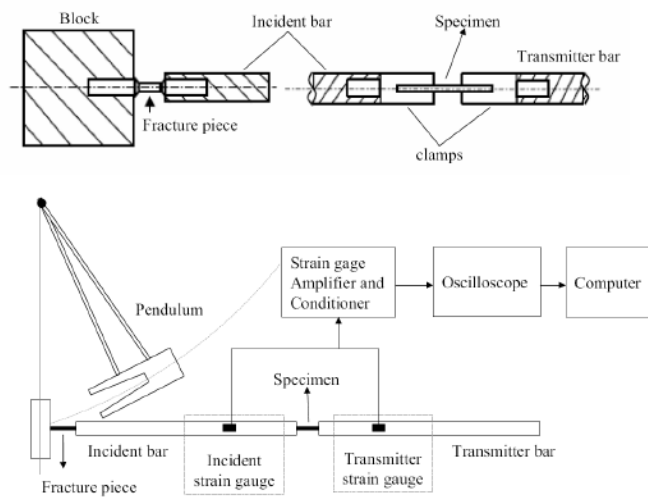


Figure 4: Schematic of the high strain rate test on a Split Hopkinson pressure bar in tension.

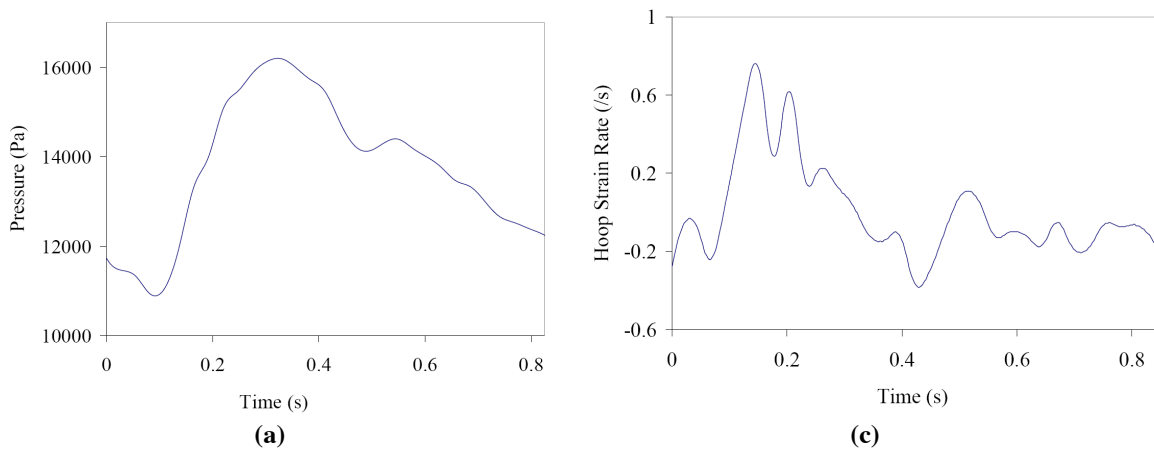


Figure 5: Numerical estimation of strain rates in the carotid artery. (a) Pressure waveform and (c) hoop strain rates.

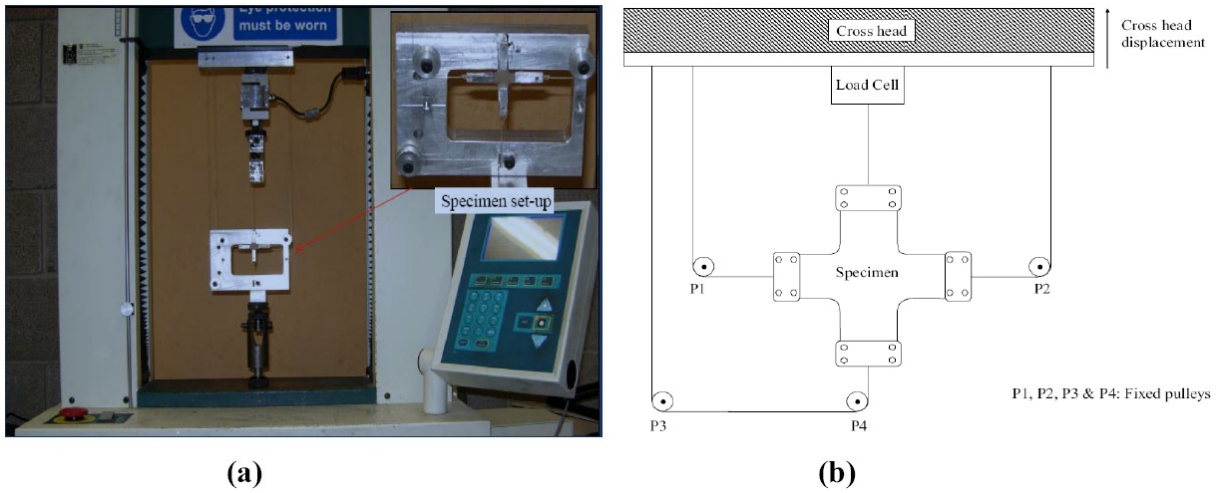


Figure 6: Biaxial (a) experimental set-up and (b) schematic drawing of experimental set-up

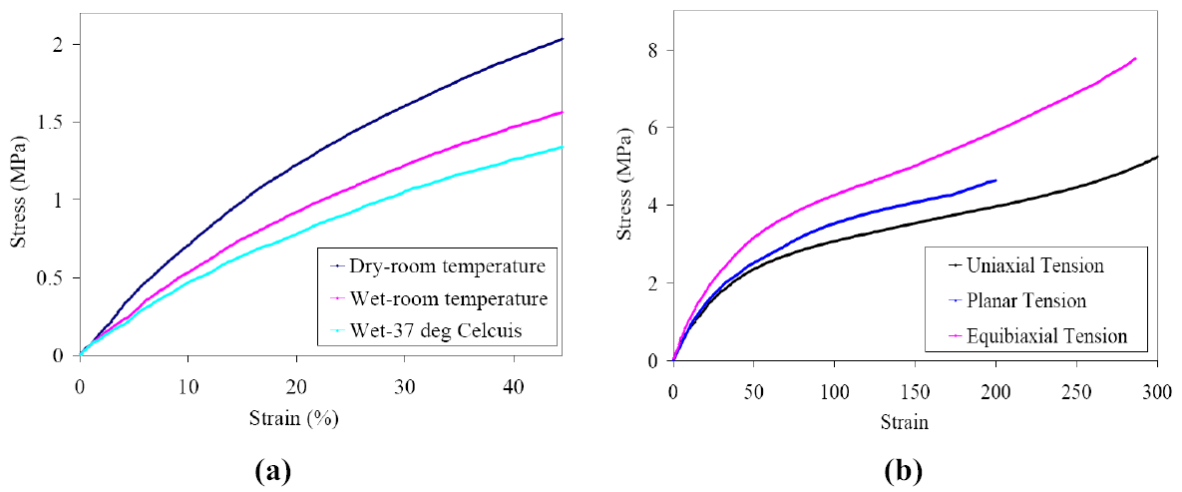


Figure 7: (a) Stress-strain behaviour of polyurethane rubber under different test conditions and (b) uniaxial, planar and equibiaxial tension stress-strain behaviour of the rubber under dry-room temperature condition, and at a strain rate of 0.013/s.

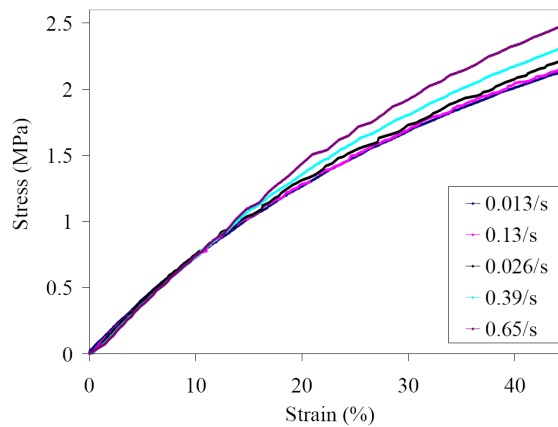
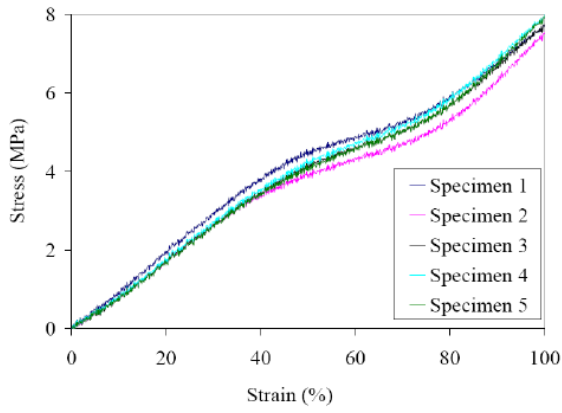
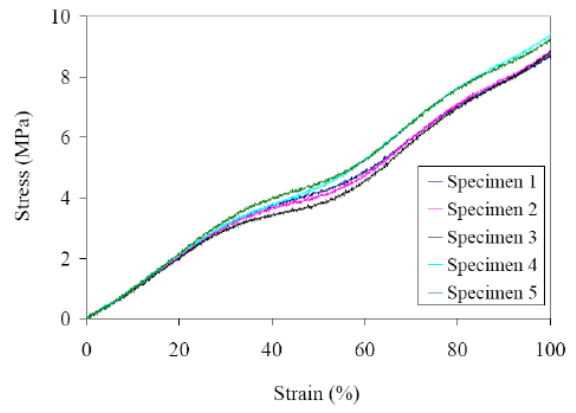


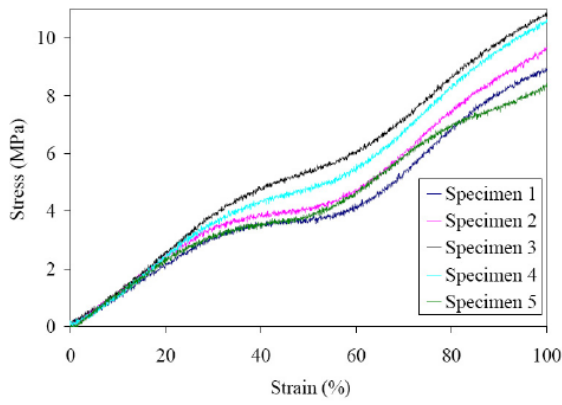
Figure 8: Strain rate dependency of polyurethane rubber at low strain rates.



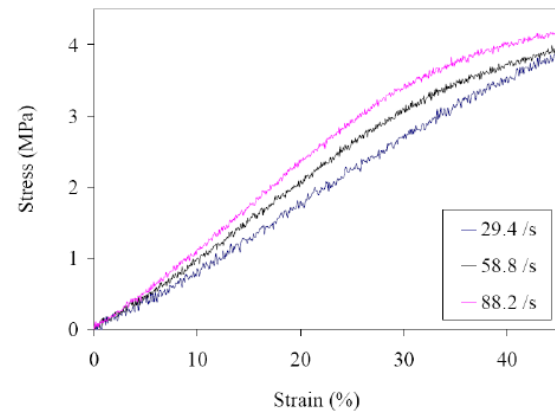
(a)



(b)



(c)



(d)

Figure 9: Intermediate strain rate uniaxial test results for (a) 29.4 /s, (b) 58.8 /s, (c) 88.2 /s strain rates and (d) the average stress-strain behaviour of polyurethane rubber at different strain rates.

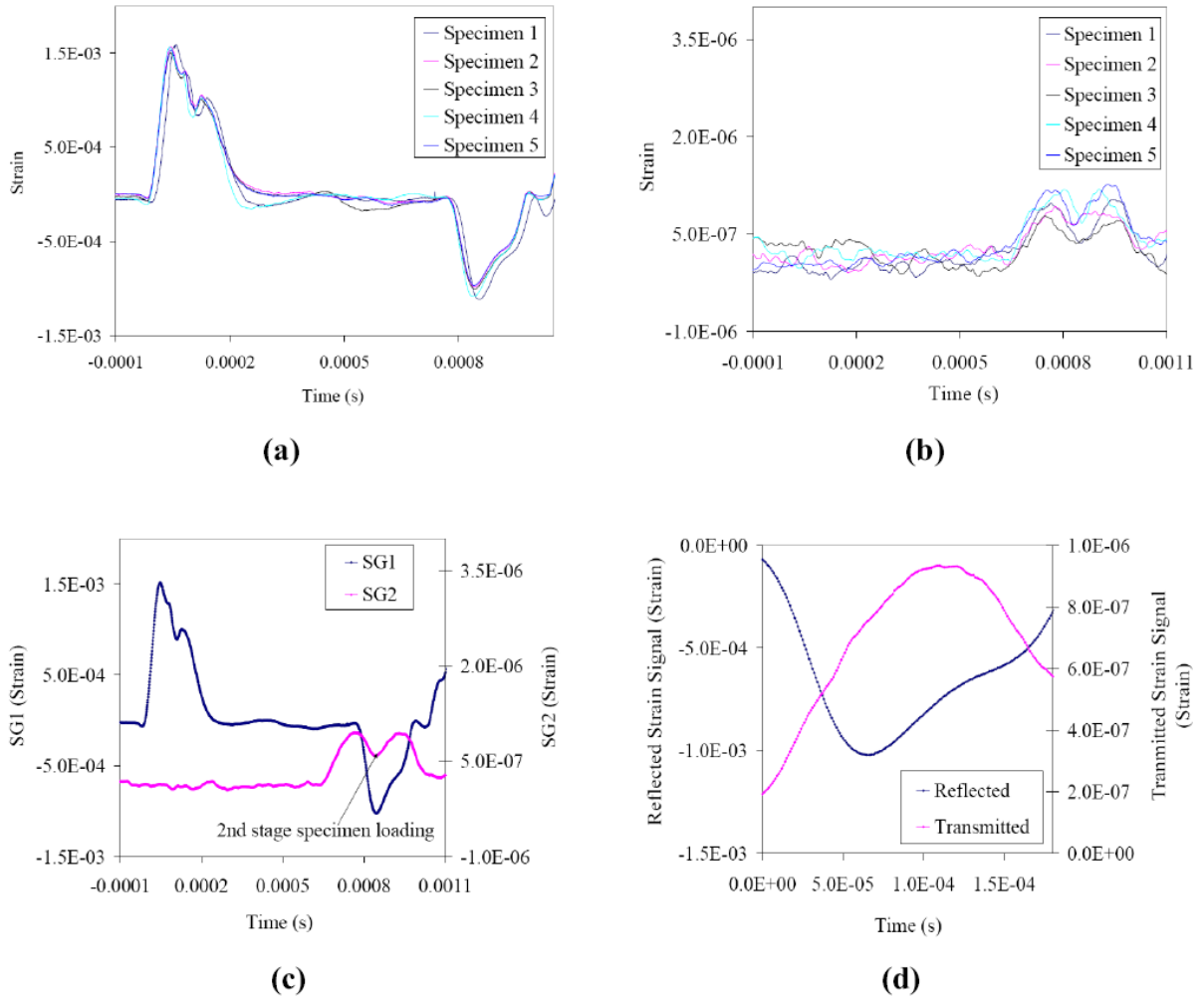


Figure 10: (a) Strain signals recorded by the incident and (b) transmitter strain gages, (c) the averaged strain signals and (d) reflected and transmitted strain signals, at a strain rate of 137.5 /s.

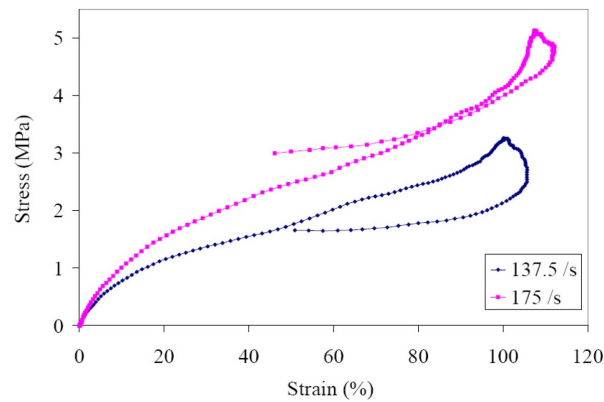


Figure 11: Stress-strain behaviour of polyurethane rubber at the strain rates of 137.5 /s and 175 /s.

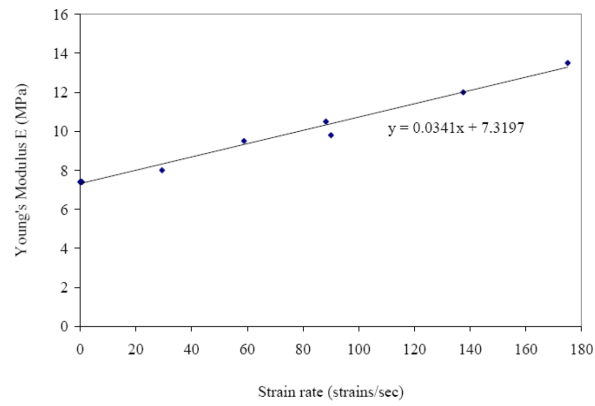
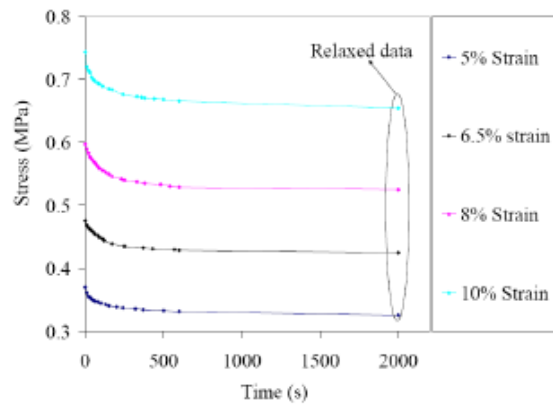
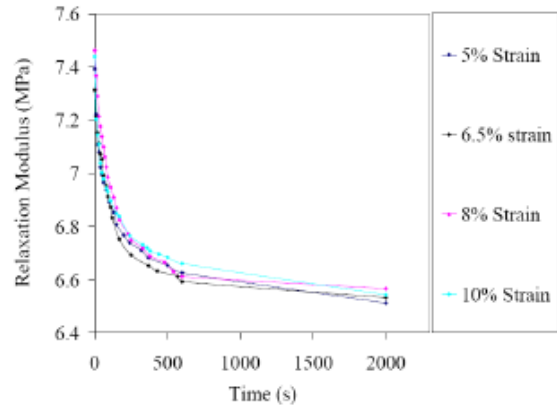


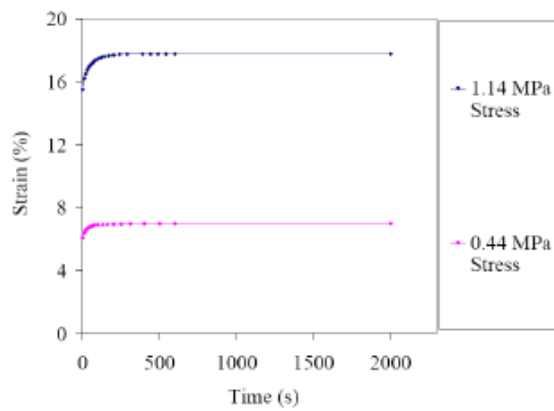
Figure 12: The Young's modulus of polyurethane rubber expressed as a function of strain rate.



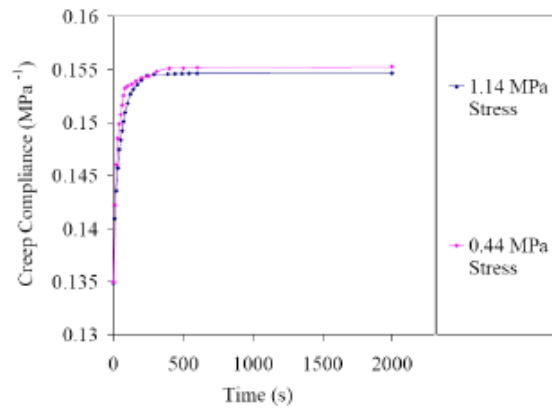
(a)



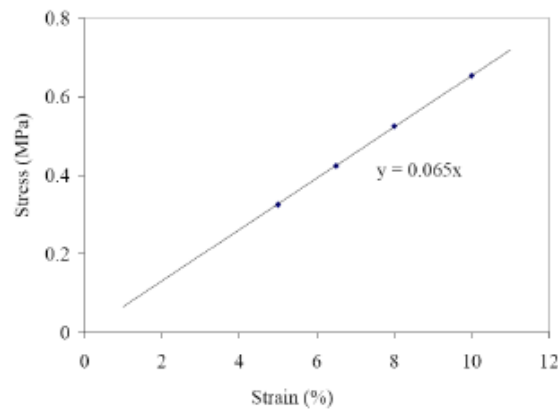
(b)



(c)

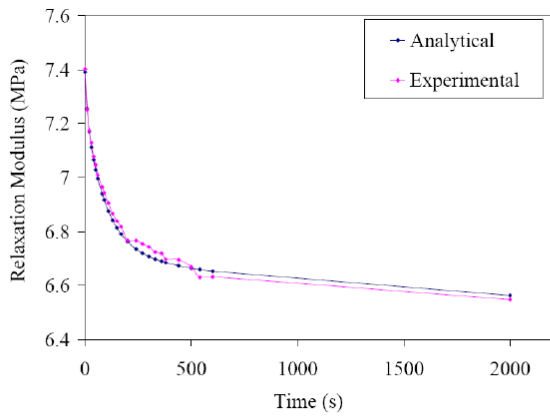


(d)

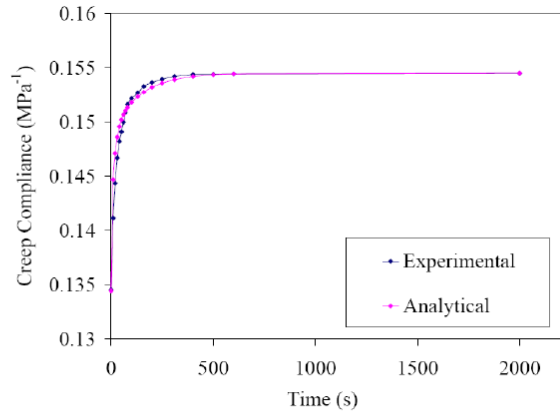


(e)

Figure 13: Viscoelastic behaviour of polyurethane rubber under dry-room temperature condition: (a) relaxation data and (b) relaxation modulus at different strain magnitudes, (c) creep data and (d) creep compliance at different stress magnitudes and (e) relaxed modulus.

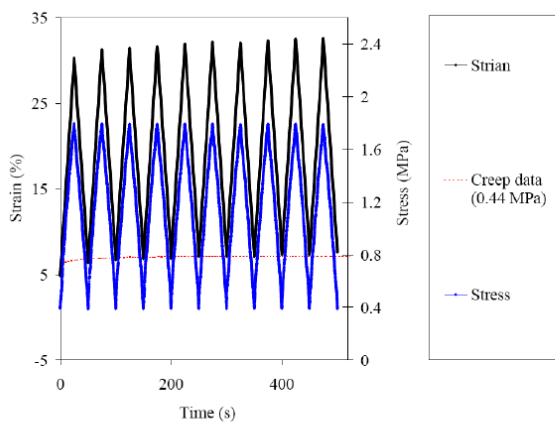


(a)

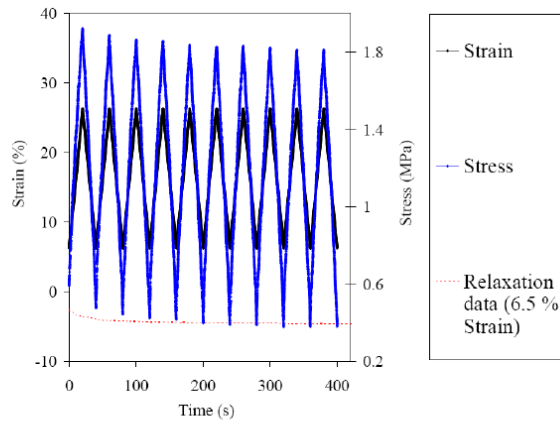


(b)

Figure 14: Viscoelastic properties of polyurethane rubber: (a) Relaxation modulus, (b) Creep compliance



(a)



(b)

Figure 15: Cyclic tests results under dry-room temperature condition; (a) material creep, with stress as the loading function, and (b) material stress relaxation, with strain as a loading function

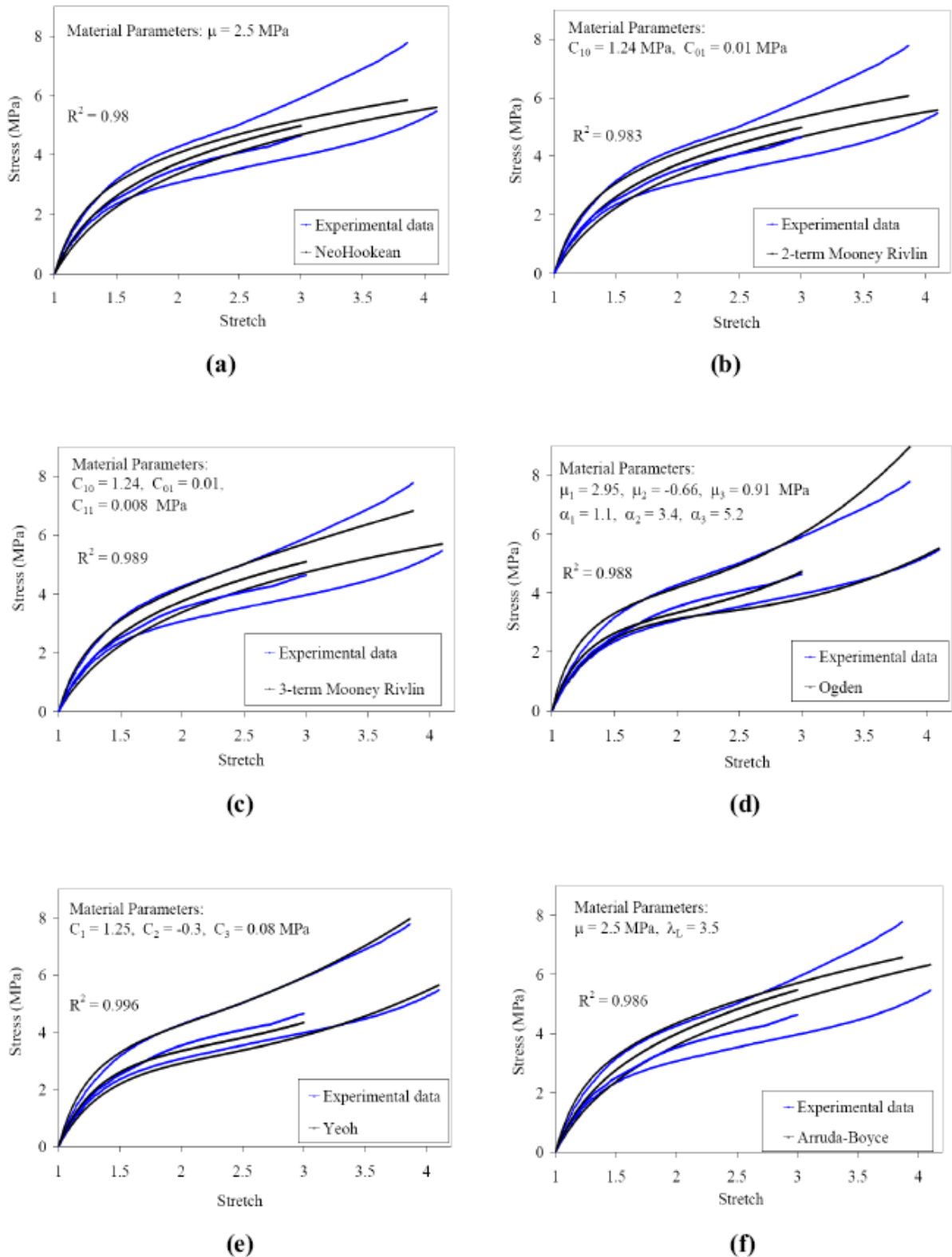


Figure 16: Comparison between experimental data and the predictions of hyperelastic material models for (a) NeoHookean, (b) 2-term Mooney Rivlin, (c) 3-term Mooney Rivlin, (d) Ogden, (e) Yeoh and (f) Arruda-Boyce material models.